Nucl. Fusion **56** (2016) 014001 (7pp) doi:10.1088/0029-5515/56/1/014001

Letter

Canonical symplectic particle-in-cell method for long-term large-scale simulations of the Vlasov–Maxwell equations

Hong Qin[1,2], Jian Liu[1,3], Jianyuan Xiao[1,3], Ruili Zhang[1,3], Yang He[1,3], Yulei Wang[1,3], Yajuan Sun[4], Joshua W. Burby[2], Leland Ellison[2] and Yao Zhou[2]

[1] School of Nuclear Science and Technology and Department of Modern Physics, University of Science and Technology of China, Hefei, Anhui 230026, People's Republic of China
[2] Plasma Physics Laboratory, Princeton University, Princeton, NJ 08543, USA
[3] Key Laboratory of Geospace Environment, CAS, Hefei, Anhui 230026, People's Republic of China
[4] LSEC, Academy of Mathematics and Systems Science, Chinese Academy of Sciences, Beijing 100190, People's Republic of China

E-mail: hongqin@ustc.edu.cn

Received 15 April 2015, revised 11 September 2015
Accepted for publication 9 October 2015
Published 2 December 2015

Abstract

Particle-in-cell (PIC) simulation is the most important numerical tool in plasma physics. However, its long-term accuracy has not been established. To overcome this difficulty, we developed a canonical symplectic PIC method for the Vlasov–Maxwell system by discretising its canonical Poisson bracket. A fast local algorithm to solve the symplectic implicit time advance is discovered without root searching or global matrix inversion, enabling applications of the proposed method to very large-scale plasma simulations with many, e.g. 10^9, degrees of freedom. The long-term accuracy and fidelity of the algorithm enables us to numerically confirm Mouhot and Villani's theory and conjecture on nonlinear Landau damping over several orders of magnitude using the PIC method, and to calculate the nonlinear evolution of the reflectivity during the mode conversion process from extraordinary waves to Bernstein waves.

Keywords: particle-in-cell simulations, Vlasov–Maxwell equations, canonical symplectic algorithm

(Some figures may appear in colour only in the online journal)

In modern plasma physics, numerically solving the Vlasov–Maxwell (VM) equations using the particle-in-cell (PIC) method has become the most important tool [1, 2] for theoretical studies in the last half century. Many innovative algorithms, such as the Boris scheme for advancing particles [3, 4] and Villasenor–Buneman's charge-conserving deposition scheme [5], have been developed and successfully applied. Recently, a new geometric numerical methodology has been adopted for PIC simulations. This exciting trend begins with the discovery of symplectic algorithms for Hamiltonian equations that govern charged particle dynamics [6–16]. The Boris algorithm was discovered to be volume-preserving [17, 18] and high-order volume-preserving methods have been found [19]. In addition, the Vlasov–Maxwell system [20–24] and

the Vlasov–Poisson system [25] have been discretised from a variational symplectic perspective that preserves symplectic structures and exhibits excellent long-term accuracy and fidelity.

In this letter, we develop a new canonical symplectic PIC method for solving the VM equations by discretising its canonical Poisson bracket [26]. The distribution function f is first discretised in phase space through the Klimontovich representation by a finite number of Lagrangian sampling points $(\mathbf{X}_i, \mathbf{P}_i)$ $(i = 1, ..., N)$, where $\mathbf{X}_i$ and $\mathbf{P}_i$ are the position and canonical momentum of the ith particle, and N is the total number of sampling points. The electromagnetic field is discretised point-wise on a given spatial grid, and the Hamiltonian functional is expressed as a function of the sampling points and the discretised electromagnetic field. This procedure generates a finite-dimensional Hamiltonian system with a canonical symplectic structure. The number of degrees of freedom for the discrete system is $D = 3N + 3M$, where M denotes the total number of discrete grid-points.

In general, for a Hamiltonian function whose momentum dependence and position dependence are not separable, it is not possible to make symplectic integration algorithms explicit [9, 14]. For the discrete Hamiltonian system developed here for the VM equations, the dimension of the system is usually very large, and root searching algorithms required by implicit methods are too time-consuming to be practical. However, we discovered that if the symplectic Euler algorithm [9] is applied to the discrete VM Hamiltonian system at hand, the implicit time advance can be carried out as inexpensively as an explicit method by just inverting a 3×3 matrix for every particle separately. The resulting canonical symplectic PIC method for the VM system inherits all the good numerical features of canonical symplectic algorithms, such as the long-term bound on energy-momentum error. Being symplectic means that the numerical solution satisfies $D(2D - 1)$ constraints as the exact solution does. Since D is a large number, the symplectic condition is much stronger than a few constraints on global energy and momentum. The symplectic condition almost implies imposing local conservation everywhere in phase space.

Two examples of application are given. In the first example, we simulate the dynamics of nonlinear Landau damping. It also serves as a test of the algorithm. The discrete VM Hamiltonian system for this study has more than 2.69×10^8 degrees of freedom. The damping rate from the numerical results agrees exactly with the theoretical result. Furthermore, long-term simulations reveal that the phase mixing dynamics in velocity space is the physical mechanism of the nonlinear Landau damping, as recently proven by Mouhot and Villani [27, 28] for the Vlasov–Poisson system and conjectured by Villani [29] for the Vlasov–Maxwell system. In the second application, we study the nonlinear mode conversion process from extraordinary modes to Bernstein modes (X-B mode conversion) in an inhomogeneous hot plasma. Simulations show that nonlinear mode excitations and self-interaction of the Bernstein waves significantly modify the reflectivity and conversion rate. It is the long-term accuracy and fidelity of the canonical symplectic PIC algorithm that enables us to numerically confirm Mouhot and Villani's theory and conjecture over several orders of magnitude using the PIC method, and to calculate the nonlinear evolution of the reflectivity during the X-B mode conversion.

We start from the canonical Poisson bracket and Hamiltonian for the Vlasov–Maxwell equations [26],

$$\{F, G\} \equiv \int f \left\{ \frac{\delta F}{\delta f}, \frac{\delta G}{\delta f} \right\}_{\mathbf{xp}} \mathrm{d}\mathbf{x}\mathrm{d}\mathbf{p} + \int \left(\frac{\delta F}{\delta \mathbf{A}} \frac{\delta G}{\delta \mathbf{Y}} - \frac{\delta G}{\delta \mathbf{A}} \frac{\delta F}{\delta \mathbf{Y}} \right) \mathrm{d}\mathbf{x}. \tag{1}$$

$$H(f, \mathbf{A}, \mathbf{Y}) = \frac{1}{2} \int (\mathbf{p} - \mathbf{A})^2 f \, \mathrm{d}\mathbf{x}\mathrm{d}\mathbf{p} + \frac{1}{2} \int [\mathbf{Y}^2 + (\nabla \times \mathbf{A})^2] \mathrm{d}\mathbf{x}. \tag{2}$$

Here, F, G and the Hamiltonian H are functionals of the distribution function f, vector potential $\mathbf{A}$ and $\mathbf{Y} \equiv \partial \mathbf{A}/\partial t$. The bracket $\{h, g\}_{\mathbf{xp}}$ inside the first term on the right-hand side of equation (1) is the canonical Poisson bracket for functions h and g of canonical phase space $(\mathbf{x}, \mathbf{p})$. The temporal gauge, i.e. $\phi = 0$, has been explicitly chosen for this Poisson bracket to be valid. The Poisson bracket defined in equation (1) can be formally derived from the point of view of co-adjoint orbit theory [26], and can be used to derive the non-canonical Morrison–Marsden–Weinstein bracket in the $(f, \mathbf{E}, \mathbf{B})$ and $(\mathbf{x}, \mathbf{v})$ coordinates [26, 30, 31]. First, we discretise the distribution function using the Klimontovich representation

$$f(\mathbf{x}, \mathbf{p}, t) = \sum_{i=1}^{N} \delta(\mathbf{x} - \mathbf{X}_i) \delta(\mathbf{p} - \mathbf{P}_i), \tag{3}$$

where $(\mathbf{X}_i, \mathbf{P}_i)$ $(i = 1, ..., N)$ are the particles' coordinates in phase space. Under this discretisation, it can be shown that

$$\frac{\delta F}{\delta \mathbf{X}_i} = \int \delta(\mathbf{x} - \mathbf{X}_i) \delta(\mathbf{p} - \mathbf{P}_i) \frac{\partial}{\partial \mathbf{x}} \left(\frac{\delta F}{\delta f} \right) \mathrm{d}\mathbf{x}\mathrm{d}\mathbf{p}, \tag{4}$$

$$\frac{\delta F}{\delta \mathbf{P}_i} = \int \delta(\mathbf{x} - \mathbf{X}_i) \delta(\mathbf{p} - \mathbf{P}_i) \frac{\partial}{\partial \mathbf{p}} \left(\frac{\delta F}{\delta f} \right) \mathrm{d}\mathbf{x}\mathrm{d}\mathbf{p}, \tag{5}$$

from which we obtain

$$\frac{\delta F}{\delta \mathbf{X}_i} \frac{\delta G}{\delta \mathbf{P}_i} - \frac{\delta G}{\delta \mathbf{X}_i} \frac{\delta F}{\delta \mathbf{P}_i} = \int \delta(\mathbf{x} - \mathbf{X}_i) \delta(\mathbf{p} - \mathbf{P}_i) \left\{ \frac{\delta F}{\delta f}, \frac{\delta G}{\delta f} \right\}_{\mathbf{xp}} \mathrm{d}\mathbf{x}\mathrm{d}\mathbf{p}. \tag{6}$$

It then follows that the first term on the right-hand side of equation (1) is

$$\int f \left\{ \frac{\delta F}{\delta f}, \frac{\delta G}{\delta f} \right\}_{\mathbf{xp}} \mathrm{d}\mathbf{x}\mathrm{d}\mathbf{p} = \sum_{i=1}^{N} \left(\frac{\delta F}{\delta \mathbf{X}_i} \frac{\delta G}{\delta \mathbf{P}_i} - \frac{\delta G}{\delta \mathbf{X}_i} \frac{\delta F}{\delta \mathbf{P}_i} \right). \tag{7}$$

A similar derivation of the discretised bracket can be found in the context of the Hamiltonian description of vortex fluid [32, 33].

To discretise the second term on the right-hand side of equation (1), we first discretise the fields $\mathbf{A}(t)$ and $\mathbf{Y}(t)$ on a Eulerian spatial grid as

$$\mathbf{A}(\mathbf{x}, t) = \sum_{J=1}^{M} \mathbf{A}_\mathbf{J}(t) \Psi(\mathbf{x} - \mathbf{x}_J), \quad \mathbf{Y}(\mathbf{x}, t) = \sum_{J=1}^{M} \mathbf{Y}_J(t) \Psi(\mathbf{x} - \mathbf{x}_J), \tag{8}$$

where the discrete fields $\mathbf{A}_J(t)$ and $\mathbf{Y}_J(t)$ are the fields evaluated on the grid-point $\mathbf{x}_J$. The subscript J is the index of the grid-point, and M is the total number of the grid-points. Here, $\Psi(\mathbf{x}-\mathbf{x}_J)$ is the step function,

$$\Psi(\mathbf{x}-\mathbf{x}_J)=\begin{cases}1, & |x-x_J|<\frac{\Delta x}{2},|y-y_J|<\frac{\Delta y}{2},|z-z_J|<\frac{\Delta z}{2},\\ 0, & \text{elsewhere.}\end{cases} \tag{9}$$

Under this discretisation of $\mathbf{A}(t)$ and $\mathbf{Y}(t)$, we have

$$\frac{\delta F}{\delta \mathbf{A}}=\sum_{J=1}^{M}\frac{\delta \mathbf{A}_J}{\delta \mathbf{A}}\frac{\partial F}{\partial \mathbf{A}_J}=\sum_{J=1}^{M}\frac{1}{\Delta V}\Psi(\mathbf{x}-\mathbf{x}_J)\frac{\partial F}{\partial \mathbf{A}_J}, \tag{10}$$

where ΔV is the volume of each cell, which is taken to be a constant in the present study. For the second equal sign in equation (10), use has been made of the fact that

$$\frac{\delta \mathbf{A}_J}{\delta \mathbf{A}}=\frac{1}{\Delta V}\Psi(\mathbf{x}-\mathbf{x}_J). \tag{11}$$

The discretisation of the second term on the right-hand side of equation (1) is thus

$$\int\left(\frac{\delta F}{\delta \mathbf{A}}\frac{\delta G}{\delta \mathbf{Y}}-\frac{\delta G}{\delta \mathbf{A}}\frac{\delta F}{\delta \mathbf{Y}}\right)\mathrm{d}\mathbf{x}=\sum_{J=1}^{M}\left(\frac{\partial F}{\partial \mathbf{A}_J}\frac{\partial G}{\partial \mathbf{Y}_J}-\frac{\partial G}{\partial \mathbf{A}_J}\frac{\partial F}{\partial \mathbf{Y}_J}\right)\frac{1}{\Delta V}. \tag{12}$$

Finally, the discrete Poisson bracket for the VM system is

$$\{F,G\}=\sum_{i=1}^{N}\left(\frac{\delta F}{\delta \mathbf{X}_i}\frac{\delta G}{\delta \mathbf{P}_i}-\frac{\delta G}{\delta \mathbf{X}_i}\frac{\delta F}{\delta \mathbf{P}_i}\right)+\sum_{J=1}^{M}\left(\frac{\partial F}{\partial \mathbf{A}_J}\frac{\partial G}{\partial \mathbf{Y}_J}-\frac{\partial G}{\partial \mathbf{A}_J}\frac{\partial F}{\partial \mathbf{Y}_J}\right)\frac{1}{\Delta V} \tag{13}$$

for functions F and G of the particles $(\mathbf{X}_i,\mathbf{P}_i)$ and the discretised field $(\mathbf{A}_J,\mathbf{Y}_J)$.

Next, we need to express the Hamiltonian functional given by equation (2) in terms of $(\mathbf{X}_i,\mathbf{P}_i)$ and $(\mathbf{A}_J,\mathbf{Y}_J)$. The particles' total kinetic energy is the sum of each particle's kinetic energy. The vector potential at a particle's position can be interpolated from $\mathbf{A}_J(t)$ as

$$\mathbf{A}(\mathbf{X}_j,t)=\sum_{J=1}^{M}\mathbf{A}_J(t)W(\mathbf{X}_j-\mathbf{x}_J), \tag{14}$$

where $W(\mathbf{X}_j-\mathbf{x}_J)$ is a chosen interpolation function. Note that $W(\mathbf{X}_j-\mathbf{x}_J)$ is not necessarily the same as the step function $\Psi(\mathbf{x}-\mathbf{x}_J)$ in equation (8). This is of course allowed as long as the consistency condition is satisfied, i.e. the continuous limit is recovered when the grid-size goes to zero. The Hamiltonian then becomes

$$\begin{aligned}\tilde{H}(\mathbf{X}_i,\mathbf{P}_i,\mathbf{A}_J,\mathbf{Y}_J)=&\frac{1}{2}\sum_{i=1}^{N}\left(\mathbf{P}_i^2-2\mathbf{P}_i\cdot\sum_{J=1}^{M}\mathbf{A}_J W(\mathbf{X}_i-\mathbf{x}_J)\right.\\ &\left.\sum_{J,L=1}^{M}\mathbf{A}_J\cdot\mathbf{A}_L W(\mathbf{X}_i-\mathbf{x}_J)W(\mathbf{X}_i-\mathbf{x}_L)\right)\\ &+\frac{1}{2}\sum_{J=1}^{M}[\mathbf{Y}_J^2+(\nabla_d\times\mathbf{A})_J^2]\Delta V,\end{aligned} \tag{15}$$

where $(\nabla_d\times\mathbf{A})_J$ is the discrete curl operator acting on the discrete vector potential evaluated at the Jth grid-point. Finally, the discrete Hamiltonian (15) and discrete Poisson structure (13) form a canonical symplectic discretisation of the original continuous Vlasov–Maxwell system. The ordinary differential equations for the canonical system are

$$\dot{\mathbf{X}}_i=\{\mathbf{X}_i,\tilde{H}\}_d=\mathbf{P}_i-\sum_{J=1}^{M}\mathbf{A}_J W(\mathbf{X}_i-\mathbf{x}_J), \tag{16}$$

$$\dot{\mathbf{A}}_J=\{\mathbf{A}_J,\tilde{H}\}_d=\mathbf{Y}_J, \tag{17}$$

$$\begin{aligned}\dot{\mathbf{P}}_i=\{\mathbf{P}_i,\tilde{H}\}_d=&\sum_{J=1}^{M}(\mathbf{P}_i\cdot\mathbf{A}_J)\nabla W(\mathbf{X}_i-\mathbf{x}_J)\\ &-\sum_{J,L=1}^{M}(\mathbf{A}_J\cdot\mathbf{A}_L)W(\mathbf{X}_i-\mathbf{x}_J)\nabla W(\mathbf{X}_i-\mathbf{x}_L),\end{aligned} \tag{18}$$

$$\begin{aligned}\dot{\mathbf{Y}}_J=\{\mathbf{Y}_J,\tilde{H}\}_d=&\sum_{i=1}^{N}\mathbf{P}_i W(\mathbf{X}_i-\mathbf{x}_J)\frac{1}{\Delta V}\\ &-\sum_{i=1}^{N}\sum_{L=1}^{M}\mathbf{A}_L W(\mathbf{X}_i-\mathbf{x}_J)W(\mathbf{X}_i-\mathbf{x}_L)\frac{1}{\Delta V}-(\nabla_d^T\times\nabla_d\times\mathbf{A})_J.\end{aligned} \tag{19}$$

This equation system consists of $6(M+N)$ equations describing the dynamics of N particles and fields on M discrete grid-points. The last term in equation (19) is defined to be

$$(\nabla_d^T\times\nabla_d\times\mathbf{A})_J\equiv\frac{1}{2}\frac{\partial}{\partial A_J}\left[\sum_{L=1}^{M}(\nabla_d\times\mathbf{A})_L^2\right]. \tag{20}$$

The notation of $\nabla_d^T\times\nabla_d\times\mathbf{A}$ indicates that the right-hand side of equation (20) can be viewed as the discretised $\nabla\times\nabla\times\mathbf{A}$ for a well-chosen discrete curl operator ∇_d. To wit, we note that the term $\nabla\times\mathbf{A}$ in the Hamiltonian is discretised using the step function $\Psi(\mathbf{x}-\mathbf{x}_J)$,

$$\nabla\times\mathbf{A}=\sum_{J=1}^{M}(\nabla_d\times\mathbf{A})_J\Psi(\mathbf{x}-\mathbf{x}_J). \tag{21}$$

As an example, we define the discrete curl operator $(\nabla_d\times\mathbf{A})_J=(\nabla\times\mathbf{A})_{i,j,k}$ to be

$$(\nabla_d\times\mathbf{A})_J\equiv\begin{pmatrix}\frac{A^3_{i,j,k}-A^3_{i,j-1,k}}{\Delta y}-\frac{A^2_{i,j,k}-A^2_{i,j,k-1}}{\Delta z}\\ \frac{A^1_{i,j,k}-A^1_{i,j,k-1}}{\Delta z}-\frac{A^3_{i,j,k}-A^3_{i-1,j,k}}{\Delta \mathbf{x}}\\ \frac{A^2_{i,j,k}-A^2_{i-1,j,k}}{\Delta \mathbf{x}}-\frac{A^1_{i,j,k}-A^1_{i,j-1,k}}{\Delta y}\end{pmatrix}, \tag{22}$$

which can be written as a linear operator on the space of $3M$-vectors as

$$\nabla_d \times \mathbf{A} = \begin{pmatrix} (\nabla_d \times \mathbf{A})_1 \\ \vdots \\ (\nabla_d \times \mathbf{A})_M \end{pmatrix} = \Gamma \begin{pmatrix} \mathbf{A}_1 \\ \vdots \\ \mathbf{A}_M \end{pmatrix}. \tag{23}$$

Here, Γ is a $3M \times 3M$ sparse matrix specifying the discrete curl operator. The partial derivative with respect to $\mathbf{A}_J$ can be expressed as

$$\frac{1}{2}\frac{\partial}{\partial \mathbf{A}_J}\left[\sum_{L=1}^{M}(\nabla_d \times \mathbf{A})_L^2\right] = \left[\Gamma^T\Gamma\begin{pmatrix} \mathbf{A}_1 \\ \vdots \\ \mathbf{A}_M \end{pmatrix}\right]_J \equiv (\nabla_d^T \times \nabla_d \times \mathbf{A})_J, \tag{24}$$

where Γ^T is the transposition of Γ. Obviously, the notation in equation (20) or (24) is meaningful for any linear discrete curl operator ∇_d.

It is clear from equations (16)–(19) that the particles and fields interact through the interpolation function $W(\mathbf{X}_i - \mathbf{x}_J)$. The function $W(\mathbf{X}_i - \mathbf{x}_L)/\Delta V$ distributes the particles' charge over the grid-points as if they are 'charged clouds' with finite size [1].

Once the canonical symplectic structure is given, canonical symplectic algorithms can be readily constructed using well-developed methods [6–13]. For a reason soon to be made clear, we adopt the semi-explicit symplectic Euler method for time advance. The symplectic Euler method for a generic canonical Hamiltonian system is

$$p^{n+1} = p^n - \Delta t \frac{\partial H}{\partial q}(p^{n+1}, q^n), \tag{25}$$

$$q^{n+1} = q^n + \Delta t \frac{\partial H}{\partial p}(p^{n+1}, q^n). \tag{26}$$

where Δt is the time step, and the superscript n in $p^n$and q^n denotes that they are the value at the n-th time step. It is implicit for p, but explicit for q. Making use of this algorithm, the iteration rules for equations (16)–(19) are

$$\frac{\mathbf{X}_i^{n+1} - \mathbf{X}_i^n}{\Delta t} = \mathbf{P}_i^{n+1} - \sum_{J=1}^{M} \mathbf{A}_J^n W(\mathbf{X}_i^n - \mathbf{x}_J), \tag{27}$$

$$\frac{\mathbf{A}_J^{n+1} - \mathbf{A}_J^n}{\Delta t} = \mathbf{Y}_J^{n+1}, \tag{28}$$

$$\begin{aligned} \frac{\mathbf{P}_i^{n+1} - \mathbf{P}_i^n}{\Delta t} &= \sum_{J=1}^{M} (\mathbf{P}_i^{n+1} \cdot \mathbf{A}_J^n)\nabla W(\mathbf{X}_i^n - \mathbf{x}_J) \\ &\quad - \sum_{J,L=1}^{M} (\mathbf{A}_J^n \cdot \mathbf{A}_L^n) W(\mathbf{X}_i^n - \mathbf{x}_J)\nabla W(\mathbf{X}_i^n - \mathbf{x}_L), \end{aligned} \tag{29}$$

$$\begin{aligned} \frac{\mathbf{Y}_J^{n+1} - \mathbf{Y}_J^n}{\Delta t} &= \sum_{i=1}^{N} \mathbf{P}_i^{n+1} W(\mathbf{X}_i^n - \mathbf{x}_J)\frac{1}{\Delta V} \\ &\quad - \sum_{i=1}^{N}\sum_{L=1}^{M} \mathbf{A}_L^n W(\mathbf{X}_i^n - \mathbf{x}_J) W(\mathbf{X}_i^n - \mathbf{x}_L)\frac{1}{\Delta V} - (\nabla_d^T \times \nabla_d \times \mathbf{A}^n)_J. \end{aligned} \tag{30}$$

These difference equations furnish a canonical symplectic PIC method for the Vlasov–Maxwell equations.

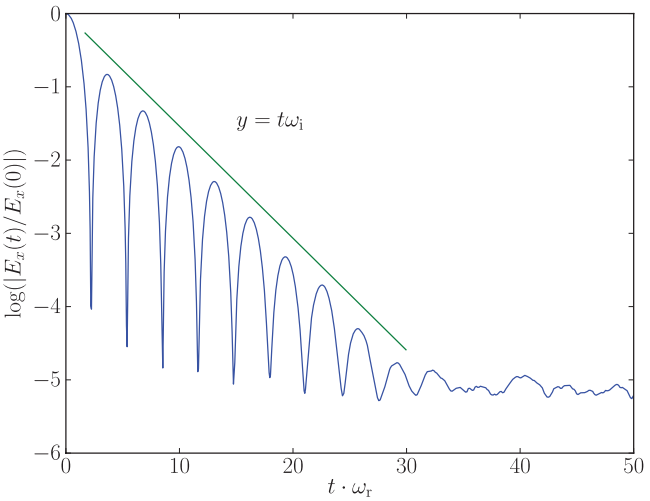

Figure 1. Perturbed electrical field as a function of time. The slope of the green line is the theoretical damping rate.

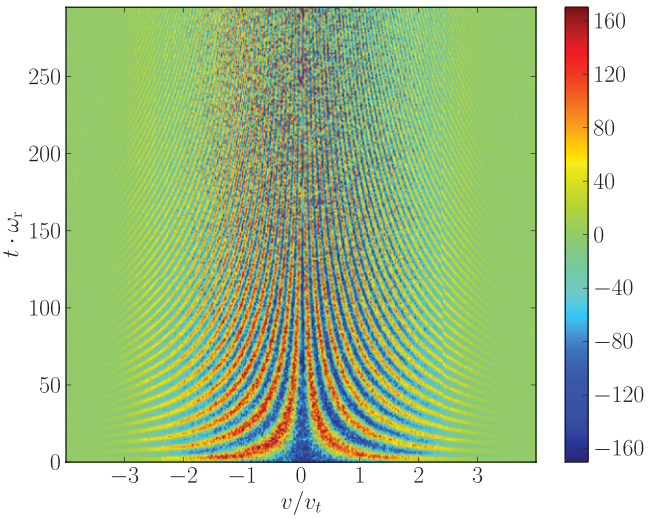

Figure 2. Electron distribution function in velocity space as a function of time. Different colours denote the amplitude of the perturbation. The mechanism of phase mixing in velocity space is clearly demonstrated. The wave-number in velocity space increases with time, which results in a decrease in density perturbation and thus attenuation of the electrical field.

As discussed above, symplectic algorithms for a Hamiltonian system with non-separable momentum and position dependence are implicit in general. This is indeed the case for the difference equations (27)–(30), because the right-hand sides of equations (27)–(30) depend on values of the $(n+1)$ th time-step. However, they are semi-explicit, because equations (27), (28) and (30) are explicit for $\mathbf{X}_i^{n+1}$, $\mathbf{A}_J^{n+1}$ and $\mathbf{Y}_J^{n+1}$, respectively. Another good property of the system is that the only implicit equation (29) is linear in terms of $\mathbf{P}_i^{n+1}$, and it is only implicit for each particle, i.e. equation (29) does not couple $\mathbf{P}_i^{n+1}$ and $\mathbf{P}_k^{n+1}$ when $i \neq k$. Therefore, the system can be solved without root searching iterations as follows. We first solve the linear equation (29) for $\mathbf{P}_i^{n+1}$ for every index i separately, which amounts to inverting a 3×3 matrix for every i. Then $\mathbf{X}_i^{n+1}$ and $\mathbf{Y}_J^{n+1}$ are advanced explicitly according to

equations (27) and (30), and the last step is to advance $\mathbf{A}_j^{n+1}$, also explicitly, according to equation (28).

The preservation of the symplectic structure exerts $D(2D-1)$ constraints on the numerical solution. Because D is a large number, preservation of symplectic structure is a very strong constraint and significantly reduces the errors of numerical solutions. We can also appreciate this advantage from the viewpoint of symplectic capacity, which is defined on any open set of the phase space. Symplectic maps preserve symplectic capacity [34], and in principle there are infinite constraints that symplectic algorithms can satisfy as the continuous systems do.

We now apply this canonical symplectic PIC scheme to simulate the nonlinear Landau damping process. This study also serves as a test of the algorithm. Previously, similar studies and tests have been performed for other algorithms, e.g. the Eulerian algorithms for the Vlasov–Poisson system [22, 35]. The ions are treated as a uniform positively charged background, and the dynamics of electrons are simulated. The electron density is $n_e = 1.149 \times 10^{16}$ m^{-3}, and the thermal velocity of electrons is $v_T = 0.1c$, where c is the light velocity in vacuum. The three-dimensional computational region is divided into $896 \times 1 \times 1$ cubic cells. The size of the grid is chosen to be $\Delta x = 2.4355 \times 10^{-4}$ m, the time step $\Delta t = \Delta x/2c$. The interpolation function is chosen to be 8th order, i.e.

$$W(\mathbf{x}) = W_1(x/\Delta x)W_1(y/\Delta x)W_1(z/\Delta x), \tag{31}$$

theoretical damping rate calculated from the dispersion relation is $\omega_i = -1.3926 \times 10^9$ s^{-1}, and the theoretical real frequency is $\omega_r = 9.116 \times 10^9$ s^{-1}. In figure 1, the slope of the green line is the theoretical damping rate and the blue curve is the evolution of the electrical field observed in the simulation. It is evident that the simulation and theory agree perfectly. After $t = 30/\omega_r$, the energy of the wave drops below the level of numerical noise, and the damping process stops. The evolution of the electron distribution function is plotted in figure 2, which clearly demonstrates the mechanism of phase mixing in velocity space. We observe in figure 2 that the wave number in velocity space increases with time, which results in a decrease in density perturbation and thus attenuation of the electrical field. More importantly, this mechanism of phase mixing is the dominant physics for the entire nonlinear evolution of the Landau damping, as proven by Mouhot and Villani [27, 28] recently for the electrostatic Vlasov–Poisson system. In addition, our simulation is electromagnetic and it shows that this physical picture of nonlinear Landau damping is also valid for the electromagnetic Vlasov–Maxwell system, as Villani conjectured [29]. It is the long-term accuracy and fidelity of the canonical symplectic PIC algorithm that enables the confirmation of Mouhot and Villani's theory and conjecture over several orders of magnitude.

Even though Mouhot and Villani rigorously proved that when the initial perturbation amplitude is small enough, the electrical perturbation will decay to zero, plasma physicists

$$W_1(q) = \begin{cases} 0, & q > 2, \\ \frac{15}{1024}q^8 - \frac{15}{128}q^7 + \frac{49}{128}q^6 - \frac{21}{32}q^5 + \frac{35}{64}q^4 - q + 1, & 1 < q \leqslant 2, \\ -\frac{15}{1024}q^8 - \frac{15}{128}q^7 + \frac{7}{16}q^6 - \frac{21}{32}q^5 + \frac{175}{256}q^4 - \frac{105}{128}q^2 + \frac{337}{512}, & 0 < q \leqslant 1, \\ -\frac{15}{1024}q^8 + \frac{15}{128}q^7 + \frac{7}{16}q^6 + \frac{21}{32}q^5 + \frac{175}{256}q^4 - \frac{105}{128}q^2 + \frac{337}{512}, & -1 < q \leqslant 0, \\ \frac{15}{1024}q^8 + \frac{15}{128}q^7 + \frac{49}{128}q^6 + \frac{21}{32}q^5 + \frac{35}{64}q^4 + q + 1, & -2 < q \leqslant -1, \\ 0, & q < -2. \end{cases} \tag{32}$$

It can be proven that the kernel function W is 3rd order continuous in the whole space. According to our performance benchmarks, this 8th-order kernel is about 30% more computationally costly than a 2nd-order kernel, which is acceptable since a higher order continuous kernel gives more numerical fidelity. Initially, 10^5 sampling points of electrons are distributed in each cell. The total number of particles is $N = 8.96 \times 10^7$, and the number of degrees of freedom is $D = 2.69 \times 10^8$. The initial electrical field perturbation is $\mathbf{E}_1 = E_1 \cos(kx)\mathbf{e}_x$, where the wave number is $k = 2\pi/224\Delta x$ and the amplitude of the perturbation electric field is $E_1 = 9.103 \times 10^4$ V m^{-1}. The simulations are performed for 80 000 time steps, during which a complete picture of the nonlinear Landau damping is revealed. As expected for symplectic algorithms, the numerical error of energy does not increase with time and is bounded within 1% for all time. The

have known this fact since the 1960s [36, 37]. It is also known that when the initial electrical perturbation is large enough, the perturbation will bounce back after initial phase of damping [36, 37]. One such case simulated is plotted in figure 3. For this case, the amplitude of the initial electrical field is 0.494 MV m^{-1} and the wave number is $k = 2\pi/272\Delta x$. Figure 4 shows the bounce-time as a function of the initial amplitude of the electrical field obtained in simulations. The physics demonstrated in our PIC simulations agrees with that obtained from Eulerian solvers [35], except that our simulations are carried out for the full Vlasov–Maxwell system.

In the second application, the 1D nonlinear mode conversion of extraordinary waves to electron Bernstein waves (X-B mode conversion) in a inhomogeneous hot plasma is simulated for a long time. The plasma density profile in the simulation is

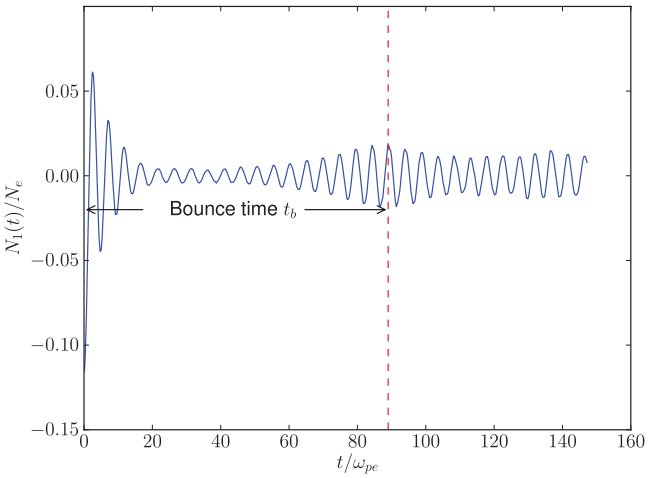

Figure 3. In nonlinear Landau damping, the perturbation will bounce back after the initial phase of damping if the initial perturbation is large enough. The amplitude of the initial electric field in this case is 0.494 MV m^{-1}.

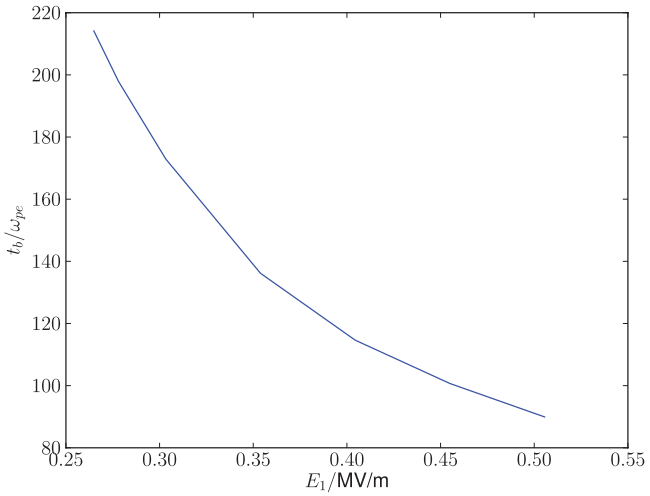

Figure 4. Relationship between the initial amplitude E_1 and the bounce time t_b in nonlinear Landau damping.

$$n_e(x) = n_0 \begin{cases} \exp\left[-\left(\dfrac{x/\Delta x - n_r - 320}{0.4 n_r}\right)^2\right], & 0 < \dfrac{x}{\Delta x} \leqslant (n_r + 320), \\ 1, & (n_r + 320) < \dfrac{x}{\Delta x} \leqslant 1300, \end{cases} \tag{33}$$

where $n_0 = 2.3 \times 10^{19}\,\mathrm{m}^{-3}$, $n_r = 380$, and $\Delta x = 2.773 \times 10^{-5}\,\mathrm{m}$ is the grid size. The thickness of the plasma boundary is $n_r \Delta x$. The electron temperature is $T_e = 57.6$ eV, and the constant external magnetic field is $\mathbf{B} = B_0 \mathbf{e}_z$ with $B_0 = 0.6$ T. The simulation domain is a $1584 \times 1 \times 1$ cubic mesh. At both boundaries in the x-direction, the Mur's absorbing condition is used, and periodic boundary conditions are adopted in the y- and z-directions. The time step is chosen to be $\Delta t = \Delta x/2c$. At the left boundary, a source is placed to excite an electromagnetic perturbation at $\omega = 0.0145/\Delta t$ with $\mathbf{E}_l = E_l \mathbf{e}_y$ and $E_1 = 900\,\mathrm{kV}$. As illustrated in figure 5, the extraordinary wave excited at the left boundary first propagates to the region of cutoff–resonance–cutoff near

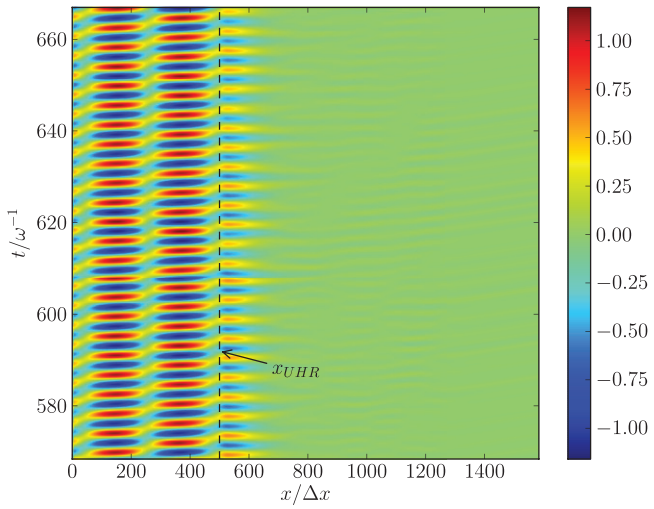

Figure 5. The space-time dependence of $E_y(t, x)$ during the nonlinear X-B mode conversion.

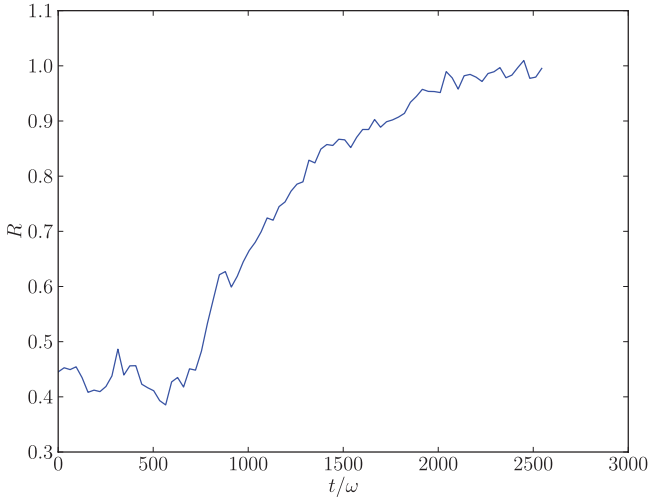

Figure 6. The evolution of reflectivity during the nonlinear X-B mode conversion.

$x/\Delta x = 500$. The wave is then partially reflected back, and partially converted into electron Bernstein waves [24]. The reflectivity evolution is plotted in figure 6. Nonlinear excitations and self-interactions of the Bernstein modes dominate the long-time dynamics of the mode conversion process. As a consequence, the reflectivity of the incident wave evolves nonlinearly, as shown in figure 6. For this set of chosen parameters, the incident wave is completely reflected at the later time of the process.

In conclusion, we have developed a canonical symplectic particle-in-cell simulation method for the Vlasov–Maxwell system by discretising its canonical Poisson bracket. In phase space, the distribution function is discretised by the Klimontovich representation using Lagrangian markers, and the electromagnetic field is discretised point-wise on a spatial grid. The resulting canonical Hamiltonian system with a large number of degrees of freedom is integrated by the symplectic Euler method, whose difference equations can be solved inexpensively by inverting a 3×3 matrix locally for every particle. Implicit root searching and global matrix inversion

are avoided entirely. This technique makes large-scale applications of the developed canonical symplectic PIC method possible. To suppress numerical noise caused by the coarse sampling, smoothing functions for sampling points can also be conveniently implemented into the canonical symplectic PIC algorithm. By incorporating the smoothing functions into the Hamiltonian functional before the discretisation, we are able to rein in all the benefits of smoothing functions without destroying the canonical symplectic structure. Progress in this and other directions will be reported in future publications.

Acknowledgments

This research is supported by the ITER-China Program (2015GB111003, 2014GB124005, 2013GB111000), the JSPS-NRF-NSFC A3 Foresight Program in the field of Plasma Physics (NSFC-11261140328), the CAS Program for Interdisciplinary Collaboration Team, the Geo-Algorithmic Plasma Simulator (GAPS) project and the US Department of Energy (DE-AC02-09CH11466).

References

[1] Birdsall C.K. and Langdon A.B. 1991 *Plasma Physics via Computer Simulation* (Bristol: Hilger)
[2] Hockney R.W. and Eastwood J.W. 1988 *Computer Simulation Using Particles* (Bristol: Institute of Physics Publishing)
[3] Boris J. 1970 *Proc. of the Fourth Conf. on Numerical Simulation of Plasmas* (Washington, DC: Naval Research Laboratory) p 3
[4] Boris J.P. 1977 Dynamic stabilization of the imploding shell rayleigh-taylor instability *Comments Plasma Phys. Control. Fusion* **3** 1
[5] Villasenor J. and Buneman O. 1992 Rigorous charge conservation for local electromagnetic field solvers *Comput. Phys. Commun.* **69** 306
[6] Ruth R.D. 1983 A canonical integration technique *IEEE Trans. Nucl. Sci.* **30** 2669
[7] Feng K. 1985 On difference schemes and sympletic geometry *The Proc. of 1984 Beijing Symp. on Differential Geometry and Differential Equations* ed K. Feng (Beijing: Science Press) pp 42–58
[8] Feng K. 1986 Difference schemes for Hamiltonian formalism and symplectic geometry *J. Comput. Math.* **4** 279–89
[9] Feng K. and Qin M. 2010 *Symplectic Geometric Algorithms for Hamiltonian Systems* (Berlin: Springer)
[10] Forest E. and Ruth R.D. 1990 4th-order symplectic integration *Physica* D **43** 105–17
[11] Channell P.J. and Scovel C. 1990 Symplectic integration of Hamiltonian systems *Nonlinearity* **3** 231–59
[12] Candy J. and Rozmus W. 1991 A symplectic integration algorithm for separable Hamiltonian functions *J. Comput. Phys.* **92** 230–56
[13] Marsden J.E. and West M. 2001 Dicrete mechanics and variational integrators *Acta Numer.* **10** 357–514
[14] Hairer E., Lubich C. and Wanner G. 2002 *Geometric Numerical Integration: Structure-Preserving Algorithms for Ordinary Differential Equations* (New York: Springer)
[15] Qin H. and Guan X. 2008 A variational symplectic integrator for the guiding center motion of charged particles for long time simulations in general magnetic fields *Phys. Rev. Lett.* **100** 035006
[16] Qin H., Guan X. and Tang W.M. 2009 Variational symplectic algorithm for guiding center dynamics and its application in tokamak geometry *Phys. Plasmas* **16** 042510
[17] Qin H., Zhang S., Xiao J., Liu J., Sun Y. and Tang W.M. 2013 Why is boris algorithm so good? *Phys. Plasmas* **20** 084503
[18] Zhang R., Liu J., Qin H., Wang Y., He Y. and Sun Y. 2015 Volume-preserving algorithm for secular relativistic dynamics of charged particles *Phys. Plasmas* **22** 044501
[19] He Y., Sun Y., Liu J. and Qin H. 2015 Volume-preserving algorithms for charged particle dynamics *J. Comput. Phys.* **281** 135
[20] Squire J., Qin H. and Tang W.M. 2012 Geometric integration of the Vlasov–Maxwell system with a variational particle-in-cell scheme *Phys. Plasmas* **19** 084501
[21] Xiao J.Y., Liu J., Qin H. and Yu Z. 2013 A variational multi-symplectic particle-in-cell algorithm with smoothing functions for the Vlasov–Maxwell system *Phys. Plasmas* **20** 102517
[22] Kraus M. 2014 Variational integrators in plasma physics *PhD Thesis*, Technical University of Munich
[23] Shadwick B.A., Stamm A.B. and Evstatiev E.G. 2014 Variational formulation of macro-particle plasma simulation algorithms *Phys. Plasmas* **21** 055708
[24] Xiao J., Liu J., Qin H., Yu Z. and Xiang N. 2015 Variational symplectic particle-in-cel simulation of nonlinear mode conversion from extraordinary waves to Bernstein waves *Phys. Plasmas*, **22** 092305
[25] Evstatiev E. and Shadwick B. 2013 Variational formulation of particle algorithms for kinetic plasma simulations *J. Comput. Phys.* **245** 376
[26] Marsden J.E. and Weinstein A. 1982 The Hamiltonian structure of the Maxwell-Vlasov equations *Physica* D **4** 394
[27] Mouhot C. and Villani C. 2011 On landau damping *Acta Math.* **207** 29
[28] Villani C. 2014 Particle systems and nonlinear landau damping *Phys. Plasmas* **21** 030901
[29] Villani C. 2014 Plasmatalks: Ron Davidson interviews Cedric Villani
[30] Morrison P.J. 1980 The Maxwell-Vlasov equations as a continuous Hamiltonian system *Phys. Lett.* A **80** 383
[31] Weinstein A. and Morrison P.J. 1981 Comments on: the Maxwell-Vlasov equaitons as a continuous Hamiltonian system *Phys. Lett.* A **86** 235
[32] Morrison P.J. 1981 Hamiltonian field description of two dimensional vortex fluids and guiding center plasmas *Technical Report* PPPL-1783, Princeton Plasma Physics Laboratory
[33] Morrison P.J. 1981 Hamiltonian field description of the one-dimensional poisson-vlasov equations *Technical Report* PPPL-1788, Princeton Plasma Physics Laboratory
[34] Hofer H. and Zehnder E. 1994 *Symplectic invariants and Hamiltonian dynamics* (Basel: Birkhäuser)
[35] Zhou T., Guo Y. and Shu C.W. 2001 Numerical study on Landau damping *Phsica* D **157** 322
[36] Armstrong T.P. 1967 Numerical studies of the nonlinear Vlasov equation *Phys. Fluids* **6** 1269
[37] Canosa J. and Gazdog J. 1974 Threshold conditions for electron trapping by nonlinear waves *Phys. Fluids* **17** 2030